

# Learning with Precise Spike Times: A New Decoding Algorithm for Liquid State Machines

**Dorian Florescu, Daniel Coca\***

Department of Automatic Control and Systems Engineering, The University of  
Sheffield, Sheffield, S1 3JD, UK.

## Abstract

There is extensive evidence that biological neural networks encode information in the precise timing of the spikes generated and transmitted by neurons, which offers several advantages over rate-based codes. Here we adopt a vector space formulation of spike train sequences and introduce a new liquid state machine (LSM) network architecture and a new forward orthogonal regression algorithm to learn an input-output signal mapping or to decode the brain activity. The proposed algorithm uses precise spike timing to select the presynaptic neurons relevant to each learning task. We show that

using precise spike timing to train the LSM and selecting the readout neurons leads to a significant increase in performance on binary classification tasks as well as in decoding neural activity from multielectrode array recordings, compared with what is achieved using the standard architecture and training method.

## 1 Introduction

It is generally accepted that neurons in the brain encode information not only in their average firing rates - rate coding - but also in the precise timing of spikes - temporal coding (Hirata et al., 2008). The importance of the precise spike timing information has been documented in many studies (Srivastava et al., 2017; Memmesheimer et al., 2014; Kayser et al., 2009; Jones et al., 2004; Gollisch & Meister, 2008; Riehle, 1997). Seth (2015) has argued that the two encoding schemes are in fact complementary.

Neuronal coding is reproducible with a precision of a millisecond (Mainen & Sejnowski, 1995; Izhikevich, 2006). It has been argued that codes that utilise spike timing make better use of the capacity of neural connections than those relying on rate codes (Mainen & Sejnowski, 1995) and that it allows processing information on much shorter time scales allowing to track rapidly changing signals (Gardner & Grüning, 2016).

There is also evidence that during perceptual decisions, learning and behaviour can be driven by a small number of neurons that are trained to read out and interpret very sparse, precisely timed action potentials (Huber et al., 2008; Houweling & Brecht, 2008; Wolfe et al., 2010).

In recent years, a lot of research effort has been expanded to establish a sound theoretical basis for encoding and decoding using the precise timing of the spikes rather

than spike-count rates (Lazar & Pnevmatikakis, 2008; Florescu & Coca, 2015; Lazar & Slutskiy, 2015; Florescu, 2017; Florescu & Coca, 2018). A range of supervised learning approaches that utilise temporal coding schemes have been developed for recurrent spiking neural networks (SNNs) with feedforward and feedback connections (Gardner & Grüning, 2016; Gütig, 2014). Some of the popular SNN training algorithms using temporal coding are based on gradient descent (Bohte et al., 2002; Xu et al., 2013; Florian, 2012; Pfister et al., 2006) or on spike timing dependent plasticity (Pfister et al., 2006; Florian, 2007; Izhikevich, 2007; Ponulak & Kasinski, 2010).

Liquid state machines (LSM) (Maass et al., 2002) are a class of recurrent SNNs that consist of a fixed high-dimensional dynamical network of biologically-realistic synapses and spiking neurons that remain unchanged during training, known as reservoir or 'Liquid', followed by a memoryless output or 'Readout' unit with adjustable synaptic weights. The Readout typically combines in a linear fashion the outputs of all the neurons in the Liquid. The LSM model can be viewed as a nonlinear dynamical system where the state vector comprises the states of all neurons in the Liquid, evolving in time according to the internal dynamics and external driving inputs, and the static Readout defines the relationship between the state vector and output (Maass et al., 2002).

The LSMs belong to the general class of reservoir computing approaches, which, compared with high-dimensional recurrent neural networks, have more biologically plausible architectures and simpler training algorithms that only tune the weights of the connections to the Readout unit (Lukosevicius & Jaeger, 2009).

The reservoir computing approaches also include non-spiking models, as the Echo

State Networks (ESNs) (Jaeger, 2001). However, the LSMs are more biologically realistic than ESNs and thus better suited for reproducing the computational properties of biological neural circuits.

The LSM Readout is typically trained by performing linear regression using the uniform samples of the filtered spike train outputs of the Liquid (Maass et al., 2002). Other proposed LSM models have feedback connections from the Readout, and are trained with recursive least squares using the filtered outputs of the Liquid (Nicola & Clopath, 2017). This leads to losing the information of the exact spike times generated by the Liquid neurons. The current training methods for LSMs learn target outputs using measurements from all the presynaptic neurons. Numerically, this model contains a large number of parameters which can lead to overfitting for large neural circuits. Moreover, it is known that projection neurons extract information only from a relatively small subset of cortical neurons that are task dependent (Häusler & Maass , 2007; Thomson et al., 2002).

In the case of ESNs, Dolinský et al. (2017) used orthogonal forward regression (OFR) to identify the contribution of each individual neuron to the response variable, and concluded that a small number of presynaptic neurons are enough to achieve accurate results.

Here we propose a new liquid state machine (LSM) architecture, and a new training algorithm that outperforms the standard method (Maass et al., 2002). The architecture consists of a Liquid, comprising only a SNN, in series with a spike time based Readout. The new algorithm, called OFR with Spike Trains (OFRST), identifies the best synaptic connectivity for the Readout unit of the LSM. The learning algorithm relies on a dis-

tance metric between two spike trains that are elements of an inner product vector space (Carnell & Richardson, 2005).

Theoretical results demonstrate that the proposed architecture can learn any continuous target output by mapping it onto a unique target spike train sequence. We prove that the proposed LSM architecture achieves higher accuracy in training compared with the standard method.

Numerical simulations are given to show the performance of the proposed method compared to the standard method for binary and multi-label input classification tasks. Additional numerical examples are used to show separately the benefit of selecting the Readout connectivity using OFR and computing with precise spike times. The advantage of the proposed method is also demonstrated for the problem of classifying the movement direction of drifting sinusoidal gratings using visually evoked multi-array recordings from the primary visual cortex of the monkey.

The paper is structured as follows. Section 2 introduces the standard architecture and method for training an LSM. Section 3 presents the proposed approach. Numerical simulations are in Section 4. Section 5 presents the conclusion.

## 2 The Standard Algorithm for Training a Liquid State Machine

A liquid state machine (LSM) is a biologically realistic spiking neural network (SNN) architecture consisting of a fixed recurrent SNN, also known as Liquid, followed by a memoryless Readout unit with adjustable synapses (Maass et al., 2002). The spike trains are elements of space  $\mathbb{S}_0$  satisfying

$$\mathbb{S}_0 = \{s | s = \{t_k\}_{k=1}^P, t_{k+1} > t_k \geq 0, \forall k = 1, \dots, P-1\}$$

The output of the Readout is a function of time  $y(t)$  satisfying (Maass et al., 2002)

$$y(t) = \mathcal{R}(\mathcal{L}\mathbf{s}^{in}),$$

where  $\mathbf{s}^{in} = [s_1^{in}, \dots, s_{N_{in}}^{in}]$  denotes the multi spike train input of the LSM,  $s_k^{in} = \{t_{k,1}^{in}, \dots, t_{k,P_k^{in}}^{in}\}$ ,  $\mathcal{L}, \mathcal{R}$  are two operators modelling the Liquid and Readout unit, respectively, satisfying  $\mathcal{L} : [\mathbb{S}_0]^{N_{in}} \rightarrow [L^2(\mathbb{R})]^N$ ,  $\mathcal{R} : [L^2(\mathbb{R})]^N \rightarrow L^2(\mathbb{R})$ , where  $N_{in}$  and  $N$  denote the number of inputs and number of neurons in the SNN, respectively.

The Liquid is represented as the composition of two mathematical operators  $\mathcal{L} = \mathcal{F}\mathcal{L}_{SNN}$ , where  $\mathcal{L}_{SNN} : [\mathbb{S}_0]^{N_{in}} \rightarrow [\mathbb{S}_0]^N$  models a generic SNN and  $\mathcal{F} : [\mathbb{S}_0]^N \rightarrow [L^2(\mathbb{R})]^N$ ,  $\mathcal{F}\mathbf{s} = [\mathcal{F}s_1, \mathcal{F}s_2, \dots, \mathcal{F}s_N]$ ,  $\forall \mathbf{s} \in [\mathbb{S}_0]^N$ ,  $\mathbf{s} = [s_1, \dots, s_N]$  models a pool of linear filters

$$\mathcal{F}s_n = \sum_{k=1}^{P_n} e^{-\frac{t-t_k^n}{\tau_s}} \cdot 1_{[t_k^n, \infty)}(t), \quad (1)$$

where  $P_n$  denotes the number of spikes in  $s_n$ ,  $1_{[t_k^n, \infty)}$  denotes the characteristic function of interval  $[t_k^n, \infty)$ , and  $\tau_s$  denotes the time constant of the filter.

The signal  $\mathbf{x}(t) = \mathcal{F}\mathcal{L}_{SNN}u(t)$  is known as the continuous state of the Liquid, satisfying  $\mathbf{x} \in [L^2(\mathbb{R})]^N$ . Maass et al. (2002) demonstrated that this model has, under idealised conditions, universal real-time computing power. The standard LSM architecture is presented in Figure 1.

**Remark 1.** *Throughout the paper, it will be assumed that  $s_k^{out} \neq s_l^{out}$ ,  $\forall k, l \in \{1, \dots, N\}$ ,  $k \neq l$ . In a practical scenario it is very unlikely that two neurons will generate two identical spike trains simultaneously. However, if this happens to be true, only the distinct outputs will be used for training.*

The most common Readout is the linear unit  $\mathcal{R}\mathbf{W}\mathbf{x}(t) = \sum_{n=1}^N w_n x_n(t)$ , where

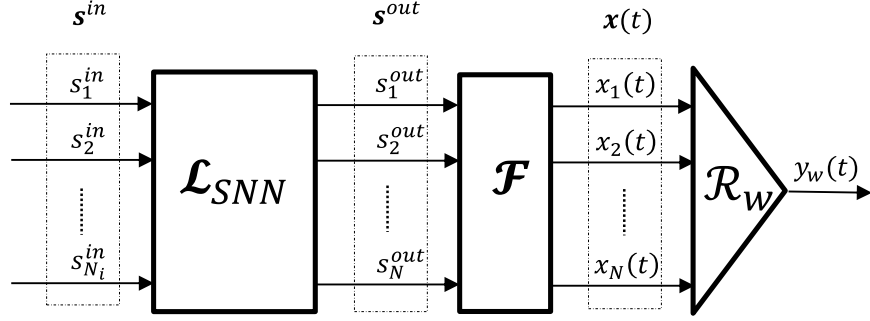


Figure 1: Block diagram of the standard architecture used for training LSMs.

$\mathbf{W} = [w_1, \dots, w_N]$  and  $\mathbf{x}(t) = [x_1(t), \dots, x_N(t)]$ . This Readout was shown to classify time-varying inputs with the same power as complex non-linear Readouts, given a large enough Liquid (Häusler et al., 2002). The weights are optimally computed using the least squares (LS) algorithm

$$\mathbf{w}_{opt} = \underset{\mathbf{w}}{\operatorname{argmin}} \|y^* - y_{\mathbf{w}}\|_{L^2}, \quad (2)$$

where  $y^* \in L^2(\mathbb{R})$  denotes the target output function,  $\|\cdot\|_{L^2}$  denotes the standard norm in  $L^2(\mathbb{R})$  and  $y_{\mathbf{w}} = \mathcal{R}_{\mathbf{w}} \mathcal{F} \mathcal{L}_{SNN} u$ .

In practice, the continuous state of the liquid  $\mathbf{x}(t)$  is sampled uniformly with period  $\Delta T > 0$ . The function  $\mathbf{x}(t)$  is not continuous in points  $\{t_k\}_{k=1}^{P_n}$  due to the expression of operator  $\mathcal{F}$  (1). Therefore  $\mathbf{x}(t)$  is not bandlimited, and thus the samples  $\{\mathbf{x}(kT)\}$  are affected by aliasing, due to Shannon's law. This leads to an incorrect evaluation of the weights  $\mathbf{w}_{opt}$  as well as an imprecise final output prediction  $y_{\mathbf{w}_{opt}}(t)$ .

Moreover, in practice not all synaptic connections of the Readout are relevant to a particular task so that training the weights of all possible connections from the Liquid neurons to the Readout can easily lead to overfitting. Furthermore, the output of the standard LSM architecture is ultimately an analog signal. Therefore the training method

is incompatible with a spike train target output.

### 3 A New LSM Training Approach using Precise Times

#### 3.1 The Proposed LSM Architecture

We propose a new spike time based Readout architecture, which does not require the bank of filters  $\mathcal{F}$  (Figure 2).

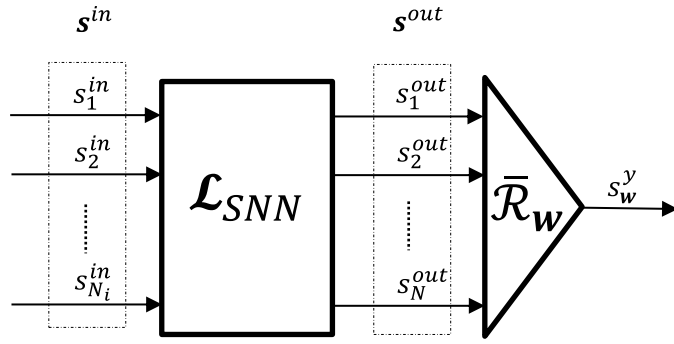


Figure 2: Block diagram of the proposed architecture used for training LSMs.

The space  $\mathbb{S}_0$  is not a linear space because it does not allow any operations between spike trains. To overcome this problem, this space is extended to the Carnell-Richardson spike train space

$$\mathbb{S} = \left\{ s = \{(a_k, t_k)\}_{k=1}^P, P \geq 1, t_k, a_k \in \mathbb{R}, t_k \neq t_l, \forall k, l \in \{1, \dots, P\}, k \neq l \right\}.$$

The space  $\mathbb{S}$  is an inner product space (Carnell & Richardson, 2005), where the standard operations are defined in Appendix 1. A spike train  $s_0 = \{t_k\}_{k=1}^P \in \mathbb{S}_0$ , as defined by the standard method, can be mapped uniquely onto an element  $s \in \mathbb{S}$ , such that  $s = \{(1, t_k)\}_{k=1}^P$ . The Readout  $\bar{\mathcal{R}}_w$  is defined using the operations in  $\mathbb{S}$  as

$$\bar{\mathcal{R}}_w s^{out} = \sum_{n=1}^{P^{out}} w_n s_n^{out} = s_w^y.$$

### 3.2 Theoretical Preliminaries

Let  $s^{y*}$  be a target spike train. Then the optimal  $\mathbf{w}$  in the least squares sense is

$$\bar{\mathbf{w}}_{opt} = \operatorname{argmin}_{\mathbf{w}} \|s^{y*} - s_{\mathbf{w}}^y\|_{\mathbb{S}},$$

where  $\|\cdot\|_{\mathbb{S}}$  denotes the standard norm in  $\mathbb{S}$ .

The proposed architecture can be extended to learn continuous target signals. To this end, the following results demonstrate that any continuous target function  $y^* \in L^2(\mathbb{R})$  can be mapped uniquely onto a spike train  $s^{y*} \in \mathbb{S}$ .

**Theorem 1.** *Let  $\mathbb{S}^{out}$  denote the subset of  $\mathbb{S}$  generated by the outputs of the SNN, such that  $\mathbb{S}^{out} = \operatorname{span}\{s_1^{out}, \dots, s_N^{out}\} \subset \mathbb{S}$ . Let  $\mathcal{F} : \mathbb{S}^{out} \rightarrow L^2(\mathbb{R})$  be an operator defined by*

$$\mathcal{F}s = \sum_{k=1}^P a_k e^{-\frac{t-t_k}{\tau_s}} \cdot 1_{[t_k, \infty)}(t), \forall s \in \mathbb{S}^{out}, s = \{(a_k, t_k)\}_{k=1}^P. \quad (3)$$

*Moreover, let  $\mathbb{FS}^{out}$  denote the subset of  $L^2(\mathbb{R})$  generated by the filtered outputs of the SNN, such that  $\mathbb{FS}^{out} = \operatorname{span}\{\mathcal{F}s_1^{out}, \dots, \mathcal{F}s_N^{out}\}$ . Then the following mapping is well defined*

$$\mathcal{M} : L^2(\mathbb{R}) \rightarrow \mathbb{S}^{out}, \mathcal{M}(y) = \mathcal{F}^{-1}\mathcal{P}_{\mathbb{FS}^{out}}(y), \forall y \in L^2(\mathbb{R}), \quad (4)$$

*where  $\mathcal{P}$  denotes the projection operator.*

*Proof.* The mapping (4) is well defined if the operator  $\mathcal{F} : \mathbb{S}^{out} \rightarrow \mathbb{FS}^{out}$  is well defined and invertible.

A function  $y \in \mathbb{FS}^{out}$  satisfies

$$y(t) = \sum_{k=1}^N w_k \mathcal{F}s_k^{out}(t) = \mathcal{F} \left( \sum_{k=1}^N w_k s_k^{out} \right) (t).$$

According to the definition of  $\mathbb{S}^{out}$  it follows that  $\sum_{k=1}^N w_k s_k^{out} \in \mathbb{S}^{out}$ , and therefore  $\mathcal{F} : \mathbb{S}^{out} \rightarrow \mathbb{FS}^{out}$  is well defined. Moreover,  $\mathcal{F}$  is invertible if it is a one-to-one and onto operator. Let  $s_1 = \sum_{k=1}^N v_k s_k^{out}$  and  $s_2 = \sum_{k=1}^N w_k s_k^{out}$ . Operator  $\mathcal{F}$  is one-to-one if

$$\mathcal{F}s_1 = \mathcal{F}s_2 \Rightarrow s_1 = s_2.$$

It follows that

$$\mathcal{F}s_1 = \mathcal{F}s_2 \Leftrightarrow \sum_{k=1}^N v_k \mathcal{F}s_k^{out}(t) = \sum_{k=1}^N w_k \mathcal{F}s_k^{out}(t) \Leftrightarrow \sum_{k=1}^N (v_k - w_k) \mathcal{F}s_k^{out}(t) = 0.$$

The functions  $\{\mathcal{F}s_k^{out}\}_{k=1}^N$  are linearly independent according to Remark 1. It follows that  $w_k = v_k, \forall k = 1, \dots, N$ , and thus  $\mathcal{F}$  is one-to-one. According to the definition of  $\mathbb{FS}^{out}$  and due to the linearity of  $\mathcal{F}$ , it follows that  $\mathcal{F}$  is also an onto operator, and thus it is invertible.

□

Theorem 1 defines a mapping that allows converting any continuous target output function  $y^*(t)$  into a unique target output spike train  $s^{y^*}$ . The operator  $\mathcal{F}$  in (3) is the extension of the filtering operator in (1) to the more general space  $\mathbb{S}$ . The following result assesses the prediction accuracy of the proposed method relative to the standard method for continuous target functions.

**Theorem 2.** *Let  $y^* \in L^2(\mathbb{R})$  and let  $\mathbf{w}_{opt}$  be the vector of weights computed for the standard architecture, such that  $\mathbf{w}_{opt} = \operatorname{argmin}_{\mathbf{w}} \|y^* - \mathcal{R}_{\mathbf{w}} \mathcal{F} \mathbf{s}^{out}\|_{L^2}$ . It follows that*

$$\mathbf{w}_{opt} = \operatorname{argmin}_{\mathbf{w}} \|s^{y^*} - \bar{\mathcal{R}}_{\mathbf{w}} \mathbf{s}^{out}\|_{\mathbb{S}} = \bar{\mathbf{w}}_{opt},$$

where  $s^{y^*} = \mathcal{M}(y^*)$ ,  $\mathcal{M}(y^*) = \mathcal{F}^{-1} \mathcal{P}_{\mathbb{FS}^{out}}(y^*)$ ,  $\mathcal{P}$  denotes the projection operator and  $\mathbb{FS}^{out} = \operatorname{span} \{\mathcal{F}s_1^{out}, \dots, \mathcal{F}s_N^{out}\}$ .

*Proof.*

$$\begin{aligned}
\|y^* - \mathcal{R}_w \mathcal{F} s^{out}\|_{L^2}^2 &= \|y^* - \mathcal{F} \bar{\mathcal{R}}_w s^{out}\|_{L^2}^2 \\
&= \|y^*\|_{L^2}^2 + \|\mathcal{F} \bar{\mathcal{R}}_w s^{out}\|_{L^2}^2 - 2 \langle y^*, \mathcal{F} \bar{\mathcal{R}}_w s^{out} \rangle_{L^2} \\
&= \|y^*\|_{L^2}^2 + \|\mathcal{F} \bar{\mathcal{R}}_w s^{out}\|_{L^2}^2 - 2 \langle \mathcal{P}_{\mathbb{F} \mathbb{S}^{out}}(y^*), \mathcal{F} \bar{\mathcal{R}}_w s^{out} \rangle_{L^2} \\
&= \|y^*\|_{L^2}^2 + \|\mathcal{F} \bar{\mathcal{R}}_w s^{out}\|_{L^2}^2 - 2 \langle \mathcal{F} s^{y*}, \mathcal{F} \bar{\mathcal{R}}_w s^{out} \rangle_{L^2} \\
&= \|y^*\|_{L^2}^2 + \frac{1}{2} \|\bar{\mathcal{R}}_w s^{out}\|_{\mathbb{S}}^2 - \langle s^{y*}, \bar{\mathcal{R}}_w s^{out} \rangle_{\mathbb{S}} \\
&= \|s^{y*} - \bar{\mathcal{R}}_w s^{out}\|_{\mathbb{S}}^2 - \|s^{y*}\|_{\mathbb{S}}^2 + \|y^*\|_{L^2}^2.
\end{aligned}$$

□

**Corollary 1.** *Theorem 2 proves that the proposed methodology achieves, in theory, the same accuracy as the state-of-the-art method when learning continuous target signals. In practice, however, the accuracy of the standard method is lower because it is affected by the sampling error introduced when calculating  $w_{opt}$  and  $y_{w_{opt}}(t)$ , which doesn't affect the proposed method.*

### 3.3 The Orthogonal Forward Regression with Spike Trains (OFRST) Algorithm

The problem addressed is to learn a target output given by a continuous function  $y^*(t)$  given a SNN of size  $N$  which generates outputs  $\{s_k^{out}\}_{k=1}^N$  in response to stimuli  $\{s_k^{in}\}_{k=1}^{N_{in}}$ . The standard method derives the optimal weights  $w_{opt}$  in the least squares sense (Maass et al., 2002). In practice, this leads to a many non zero weights that are not particularly relevant for the learning task and overfit the data.

Theorem 1 demonstrates that the problem addressed here can be reduced to learning a target spike train  $s^{y*}$ , uniquely derived from the continuous target  $y^*(t)$ . This leads

to a more precise estimation of weights  $\mathbf{w}_{opt}$ , by avoiding the sampling error (Theorem 2). Here we introduce a greedy selection algorithm for the spike trains that are most relevant for the learning task, called Orthogonal Forward Regression with Spike Trains (OFRST). The OFRST algorithm, inspired by the orthogonal forward regression (OFR) for finite dimensional spaces (Chen et al., 1989), is applied here for the infinite dimensional inner product space  $\mathbb{S}$  as follows.

Initially, let  $s_k^{\perp(1)} = s_k^{out}, \forall k = 1, \dots, N$ , be the complete set of SNN outputs. The most significant spike train  $s_{\ell_1}^{out}$  is defined as the one that maximises  $ERR_k^{(1)}$ , where  $ERR_k^{(i)}$  denotes the error-reduction-ratio (ERR) of term  $k$  at iteration  $i$ , defined as

$$ERR_k^{(i)} = \frac{\left\langle s_k^{\perp(i)}, s^{y*} \right\rangle_{\mathbb{S}}^2}{\|s_k^{\perp(i)}\|_{\mathbb{S}}^2 \cdot \|s^{y*}\|_{\mathbb{S}}^2}.$$

Subsequently, the set  $\{s_k^{\perp(2)}\}_{k=1, k \neq \ell_1}^N$  is computed by orthogonalising the remaining output spike trains against  $s_{\ell_1}^{out}$  using the Gram-Schmitt routine.

The process continues iteratively. At every iteration  $i$ , the algorithm selects the next most significant spike train  $s_{\ell_i}^{out}$  such that  $\ell_i = \operatorname{argmax}_k (ERR_k^{(i)})$ , and generates the set  $\{s_{\ell_1}^{out}, \dots, s_{\ell_i}^{out}\}$  of significant SNN outputs and the corresponding vector of weights  $\mathbf{w}^{(p)}$ . Subsequently, the set  $\{s_k^{\perp(i)}\}_{k=1, k \neq \ell_1, \dots, \ell_i}^N$  is computed from the remaining spike trains through orthogonalisation. The process continues until  $p = N$ . The final number of presynaptic neurons is selected as the smallest  $p$  that leads to the maximum prediction accuracy on the validation dataset. The detailed algorithm is given in Appendix 2.

## 4 Numerical examples

The proposed new Readout and associated training algorithm is evaluated in comparison with the standard architecture trained with least squares. Additional numerical exam-

ples show the advantage of the proposed spike based Readout, as well as the advantage of selecting the Readout presynaptic neurons using OFR. The benefit of the proposed method is also demonstrated for a multi-label classification problem using multi-array recordings from the primary visual cortex of the monkey.

The LSM Liquid consists of 240 leaky integrate-and-fire neurons, 20% of which were randomly selected to be inhibitory (Maass et al., 2002). The neurons are spatially organised as a lattice with dimensions 15x4x4. The connection probability between neurons  $a$  and  $b$  is defined as  $C \cdot e^{-(D(a,b)/\lambda)^2}$ , where  $D(a, b)$  denotes the Euclidian distance between the neurons,  $\lambda = 2$  is a parameter that controls the average number of connections and the average distance between neurons, and  $C$ , depending on whether the neurons are excitatory (E) or inhibitory (I), is 0.3 (EE) , 0.2 (EI) , 0.4 (IE) , 0.1 (II) (Maass et al., 2002). The synaptic transmission is given by the dynamic model proposed in (Markram, Wang & Tsodyks, 1998). The input is injected into 30% randomly chosen neurons in the Liquid with an input gain of 0.1. For the standard Readout architecture, the time constant of the exponential filters is  $\tau_s = 30\text{ms}$  (Maass et al., 2002).

**Example 1. Binary classification - comparison with the standard Maass algorithm.**

This example compares the performance achieved by a standard LSM with the Readout parameters estimated using least squares with that of a LSM comprising a spike-based Readout trained using the proposed OFRST method. The task is to discriminate between two spike train templates using the SNN responses. The templates are two instances of a Poisson point process with rate 20  $Hz$ , depicted in Figure 3.

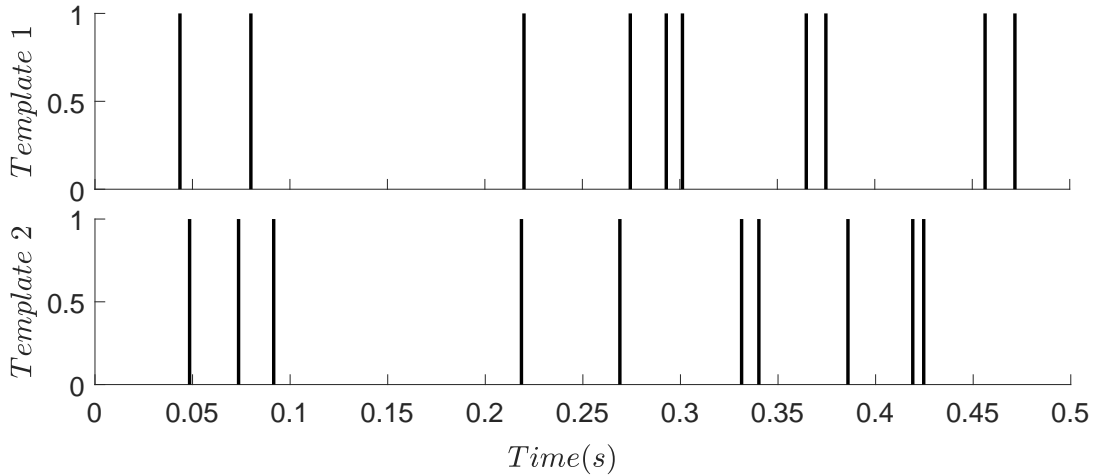


Figure 3: The input templates used for classification, generated as Poisson spike trains with frequency 20 Hz.

The inputs are generated in time interval  $[0, 0.5 s]$  by jittering one of the two templates, where the jitter noise is drawn from the Gaussian distribution with zero mean and standard deviation 6 ms. A number of 100 jittered templates were generated for each class, of which 50 were used for training and 50 for validation. The two classes of inputs are assigned the target output labels  $y(t) = 1$  (template 1) and  $y(t) = -1$

(template 2),  $t \in [0, 0.5 \text{ s}]$ . The input-output mappings are learned with the LSM by estimating the standard and proposed spike time based Readout parameters using least squares and OFRST, respectively, where the sampling time for least squares is  $\Delta T = 20$  ms (Maass et al., 2002).

In this example the classification accuracy achieved by the standard and proposed new method is 87% and 93%, respectively. In the first case, 97 out of 240 parameters of the linear Readout are different from zero, that is, the Readout processes information from 97 neurons in the liquid. In the second case only 26 neurons in the Liquid are selected by the OFRST algorithm which leads to an improved performance.

The performance of the OFRST algorithm for each iteration, computed on the validation dataset, is depicted in Figure 4. The algorithm stops after 97 iterations because none of the remaining neurons offer any additional improvement in learning the target output. The results show that when using more than 30 Readout presynaptic connections, or equivalently training for more than 30 iterations, the accuracy drops from 93% to 91%. This suggests that more than 30 Readout parameters lead to overfitting the data. This result mimics what has been observed experimentally in cortical circuits, where projection neurons extract information only from a relatively small subset cortical neurons that are task dependent (or specific) (Thomson et al., 2002; Häusler & Maass , 2007). When using all 97 presynaptic connections, the OFRST algorithm is still more accurate than the standard method by Maass et al. (2002), as pointed out in Corollary 1.

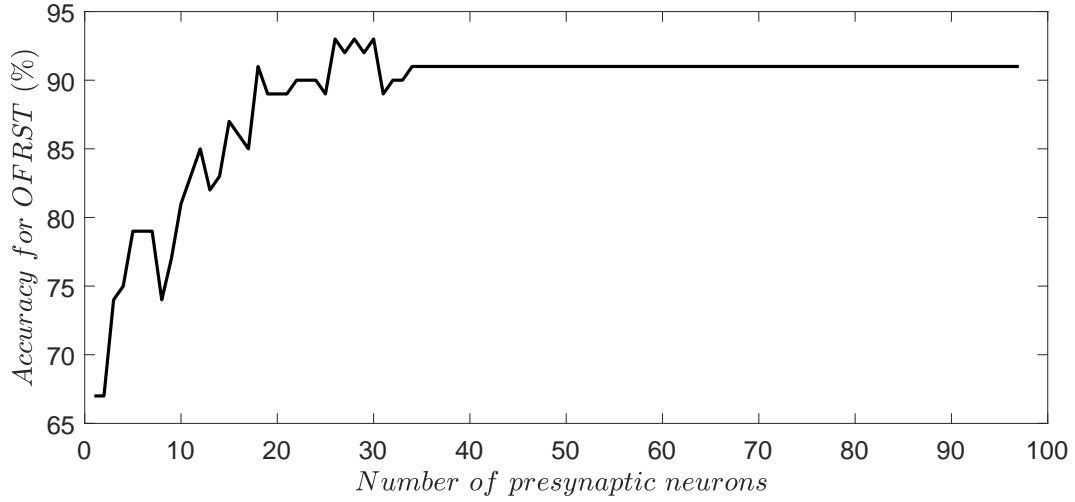


Figure 4: Accuracy of the OFRST method for each training iteration, computed on the validation dataset.

**Example 2. Binary classification - benefits of learning with exact spike times.**

In this example we compare the classification accuracy of the proposed Readout trained with the OFRST method to that of the standard Readout trained with least squares and classical OFR (Billings et al., 1989) on the same binary classification task as in Example 1.

The training and validation datasets were generated as in Example 1. For the OFR and OFRST methods the number the presynaptic neurons, which represent the regressors in the standard OFR algorithm (Billings et al., 1989), is the smallest number that achieves maximum accuracy on the validation dataset. The sampling time for the classical OFR and least squares is  $\Delta T = 20$  ms as in (Maass et al., 2002). The results for ordinary least squares, OFR and OFRST are summarised in Table 1.

Table 1: Binary classification results for least squares, standard OFR and OFRST with a pool of 240 neurons.

Training method	Total number of synapses	Accuracy
Least squares	51	77%
OFR	19	86%
OFRST	3	90%

In order to evaluate the effect of the sampling time  $\Delta T$  on the performance of the least squares and OFR algorithms, the training was performed for several sampling times ranging from 5ms to 30ms. The accuracies of the least squares and OFR algorithms, as a function of the sampling time, are depicted in Figure 5.

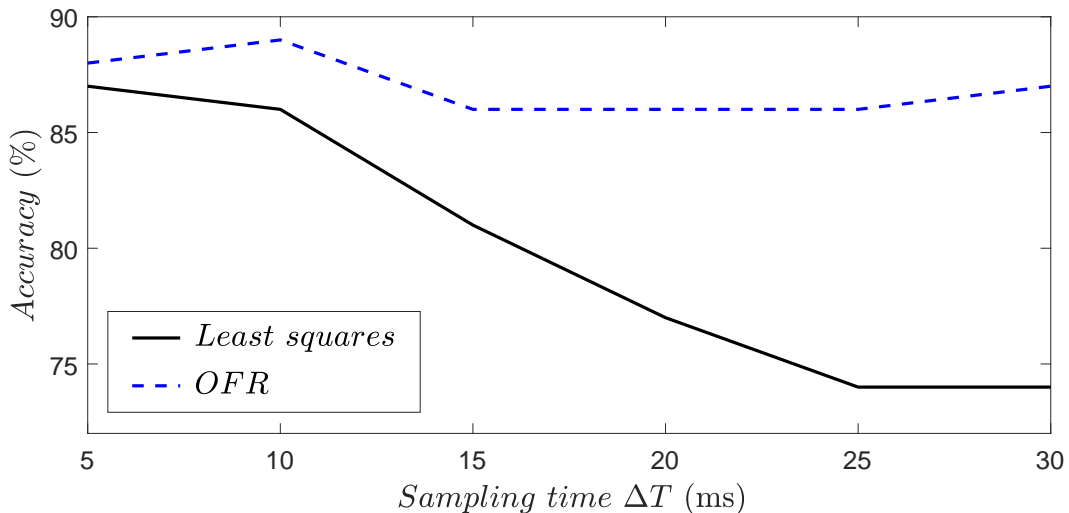


Figure 5: Accuracy computed for the least squares and OFR methods for different values of the sampling time  $\Delta T$ .

The results show that the classification accuracy for the least squares and standard OFR methods can be increased by selecting a subset of the presynaptic connections to

the Readout or decreasing the sampling time, but the performance is still below the one achieved by the OFRST method, which selects of presynaptic connections using the exact spike times generated by the Liquid neurons.

**Example 3. Binary classification: selecting relevant presynaptic neurons.**

This numerical example evaluates the performance of the OFRST in selecting the relevant presynaptic partners using exact spike timing. The SNN used in this example has a reservoir consisting of two sub-networks that are disconnected from one another, each sub-network consisting of a different pool of 240 spiking neurons generated as in examples 1 and 2. Two templates were generated as Poisson spike trains with frequency of 20 Hz over interval  $[0, 0.5\text{s}]$ . The first pool  $R_1 = \{r_1, \dots, r_{240}\}$  receives 200 inputs generated by jittering the two spike train templates, 100 for each class, of which 50 were used for training and 50 for validation, where the jitter noise is drawn from the Gaussian distribution with zero mean and standard deviation 1 ms. The second pool  $R_2 = \{r_{241}, \dots, r_{480}\}$  receives a number of 200 new jittered inputs generated from the same two templates but in a different order selected at random.

The task is to classify the inputs to sub-network  $R_1$  using the neuron outputs from the full reservoir. The OFRST algorithm is compared with the least squares and the OFR algorithms, which use the standard filtered spike train outputs.

In essence, when solving the binary classification problem, the algorithms should only select neurons from  $R_1$  as pre-synaptic partners of the Readout unit. The training results for least squares, OFR, and OFRST are summarised in Table 2.

The results show that both OFRST and OFR achieve 100% accuracy with far fewer

Table 2: Binary classification results for least squares, standard OFR and OFRST using two unconnected sub-networks with 240 neurons each.

Training method	Total number of synapses	Synapses to sub-network $R_1$	Accuracy
Least squares	217	82	96%
OFR	7	6	100%
OFRST	5	5	100%

Readout presynaptic connections than the network trained using least-squares. However, the OFR selects two additional presynaptic connections and achieves the same classification accuracy. Moreover, both the OFR and least squares algorithms select Readout presynaptic neurons from sub-network  $R_2$ , which receives jittered inputs belonging an incorrect sequence of templates.

**Example 4. Motion direction decoding using multi-electrode array recordings from the primary visual cortex.**

Here we use the proposed methodology to decode stimulus features using simultaneous multi-electrode array recordings of visually evoked activity from the primary visual cortex of three anesthetized macaque monkeys. The data were downloaded from the CRCNS online database (Kohn & Smith, 2016). Here we use the recordings from monkey number 1.

The stimuli were full-contrast drifting sinusoidal gratings at 12 orientations spaced equally ( $0^\circ, 30^\circ, 60^\circ, \dots, 270^\circ$ ). Each stimulus was presented 200 times, for a duration of 1.3 s per trial (Smith & Kohn, 2008; Kelly et al., 2010). The spiking train responses of 106 neurons were simultaneously recorded using a Utah multi-electrode array and

spike-sorted offline (Smith & Kohn, 2008; Kelly et al., 2010). In this example we only use the first 200 ms from all recording trials, which is the time reported for visual categorisation tasks in primates (Fabre-Thorpe, 1998; Hung et al., 2005). A recording trial for the  $0^\circ$  drifting bar stimulus is depicted in Figure 6.

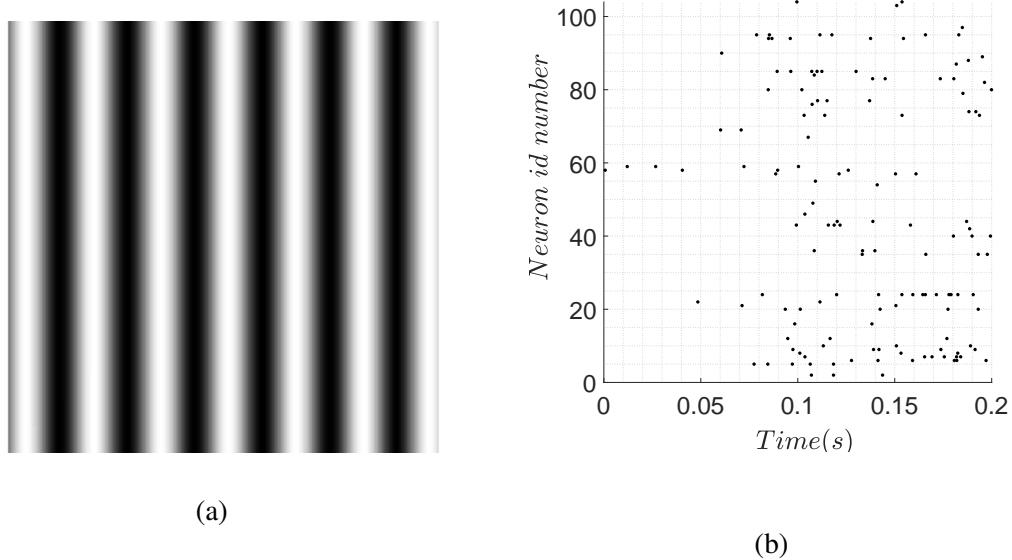


Figure 6: The first sweep of experimental data used in Example 4: a) The first frame of a drifting bar stimulus oriented at  $0^\circ$ , b) Raster plot showing the response of 106 neurons.

The decoding task is to predict the stimulus orientation based on the recorded neural activity. The task is formulated as a multi-label classification problem. Each of the 12 directions was assigned a target label (1 – 12) and a Readout. Each Readout processes the outputs of the 106 recorded neurons, which play the role of the Liquid spike train outputs.

The data (2400 trials) was randomly divided into equal datasets for training and validation, such that each dataset comprises 100 trials with each of the 12 inputs. The 12 Readouts were trained using the "one-to-all" method. Specifically, the target output for

each Readout satisfies  $y^*(t) = 1$  when the input direction label matches the Readout label, and  $y^*(t) = -1$  for any other direction. The overall prediction is given by the label of the Readout with maximum activation. The training data for each Readout consists of 100 trials from the target class and 100 trials evenly distributed among all other classes. The parameters of the 12 Readouts were tuned using ordinary least squares and the OFRST method. Considering the large number of possible connections, here the OFRST algorithm for each Readout was stopped when the criterion  $ERR_p < \zeta$  was met, where  $\zeta = 4 \cdot 10^{-4}$  is a parameter determined using a line search and  $ERR$  denotes the error reduction ratio (see Appendix 2). Essentially, this means that each Readout only connects to presynaptic neurons whose outputs contribute more than 0.04% to the variance change in the target output.

We compared the decoding performance with standard Readouts, trained with ordinary least-squares, to the performance with spike time based Readouts, trained with the OFRST algorithm described in subsection 3.3. The results are summarised in tables 3 and 4.

Table 3: Multi-label classification accuracies for the standard least squares (LS) method and the proposed OFRST method.

Training method	Readout accuracy (%)												Final accuracy
	1	2	3	4	5	6	7	8	9	10	11	12	
LS	86	84	83	81	82	84	85	83	84	87	80	78	58.17%
OFRST	88	88	86	86	84	86	88	86	85	89	82	84	67.58%

The results show that the proposed spike time based Readout, trained with the OFRST algorithm, performs significantly better than the standard Readout architecture

Table 4: Number of presynaptic connections selected for each Readout with the standard least squares (LS) method and the proposed OFRST method.

Training method	Readout connections											
	1	2	3	4	5	6	7	8	9	10	11	12
LS	106	106	106	106	106	106	106	105	105	106	106	106
OFRST	49	61	63	61	66	59	58	61	60	60	61	59

trained with least squares, while using significantly fewer neuron connections. Additionally, the proposed method also outperforms the standard algorithm for all individual binary classification tasks.

## 5 Conclusions

This work proposed a spike based Readout architecture for LSMs and introduced a new training method that uses the exact spike timing information generated by SNN models, or recorded during experimental procedures. The new method implements an orthogonal forward regression algorithm for training the Readout parameters, which exploits a distance metric defined in a spike train space.

The new algorithm, called orthogonal forward regression with spike trains (OFRST), allows the selection of the connectivity between the Liquid and the Readout unit, i.e., the neurons in the Liquid that are particularly relevant for solving a given learning or decoding task.

One advantage is that computations are carried out directly on spike trains rather than on sampled filter outputs. It is demonstrated theoretically and shown through numerical simulations, with synthetic and experimental data, that the classification accuracy is improved by using exact spike times.

Specifically, new theoretical results demonstrated that the proposed Readout trained with OFRST outperforms the standard Readout, which combine linearly the uniform samples from the neuron filtered outputs and is trained with ordinary least squares. Numerical simulations with synthetic data confirmed the theoretical findings and also showed that the proposed algorithm leads to a much smaller number of Readout synapses. A numerical study showed that OFRST outperforms the standard method on decoding the orientation of drifting gratings using the multi-electrode array recordings of the

evoked activity in the primary visual cortex of the monkey.

It is interesting to highlight the fact that typically around less than 10% of the total possible connections between Liquid and Readout are required, and that fully connected Readouts achieve less accuracy on classification tasks. This suggests that, besides decoding stimulus features from the evoked brain activity, the new training method could also be used to characterise the functional specificity of neurons in the brain.

## Appendix 1. The Carnell-Richardson Spike Train Algebra

The Carnell-Richardson spike train vector space is defined by (Carnell & Richardson, 2005)

$$\mathbb{S} = \{s = \{(a_k, t_k)\}_{k=1}^M, M \geq 1, t_k, a_k \in \mathbb{R}, \forall k = 1, \dots, M\}. \quad (5)$$

Carnell & Richardson (2005) have proven that  $\mathbb{S}$  is an inner product space, where the vector sum, scalar multiplication and inner product of two spike trains  $s_1, s_2 \in \mathbb{S}$  are defined as

$$s_1 + s_2 = \{(a_k^1, t_k^1)\}_{k=1}^{M_1} \cup \{(a_k^2, t_k^2)\}_{k=1}^{M_2},$$

$$\alpha \cdot s = \{(\alpha \cdot a_k, t_k)\}_{k=1}^M, \forall \alpha \in \mathbb{R},$$

$$\langle s_1, s_2 \rangle_{\mathbb{S}} = \sum_{k_1=1, k_2=1}^{k_1=M_1, k_2=M_2} a_{k_1}^1 a_{k_2}^2 \cdot e^{-\frac{|t_{k_1}^1 - t_{k_2}^2|}{\tau_s}},$$

where  $\tau_s > 0$  is a scaling factor.

An important subset of  $\mathbb{S}$ , which does not form a linear space, is the set  $\mathbb{S}_0$  of all possible spike trains generated by a neuron, defined as

$$\mathbb{S}_0 = \{s = \{(1, t_k)\}_{k=1}^M, M \geq 1, t_k \in \mathbb{R}, \forall k = 1, \dots, M\}.$$

Maass et al. (2002) have defined a metric  $d$  on  $\mathbb{S}_0$

$$d(s_1, s_2) = \int_{\mathbb{R}} [(\mathcal{F}s_1)(t) - (\mathcal{F}s_2)(t)]^2 dt,$$

where  $\mathcal{F} : \mathbb{S}_0 \rightarrow L^2(\mathbb{R})$ ,  $\mathcal{F}s = \sum_{k=1}^P e^{-\frac{t-t_k}{\tau_s}} \cdot 1_{[t_k^n, \infty)}(t)$  denotes the output of a linear filter with exponential decay and time constant  $\tau_s$ , given spiking input  $s$ . The inner product  $\langle \cdot, \cdot \rangle_{\mathbb{S}}$  generates a norm  $\|\cdot\|_{\mathbb{S}}$  that relates to metric  $d$  as follows  $\|s_1 - s_2\|_{\mathbb{S}} = 2d(s_1, s_2), \forall s_1, s_2 \in \mathbb{S}_0$ .

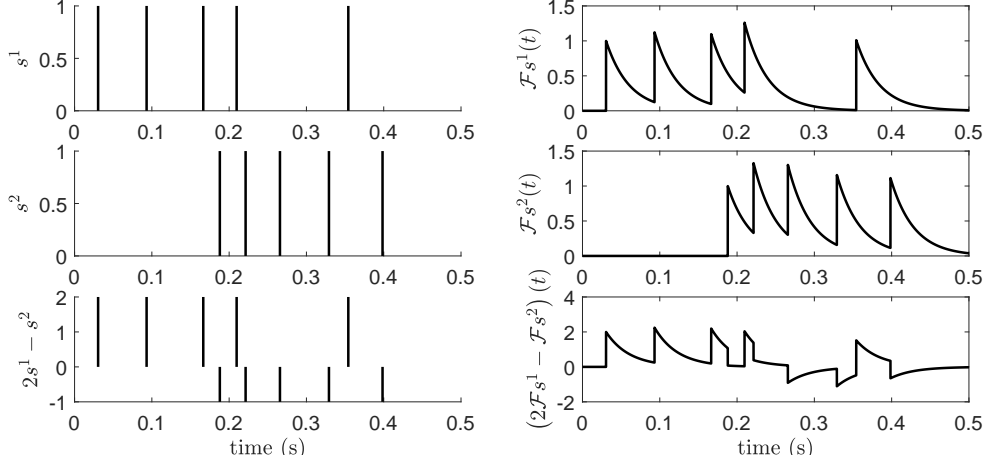


Figure 7: A linear operation between two spike trains and their postsynaptic potentials.

## Appendix 2. The Orthogonal Forward Regression with Spike Trains Algorithm (OFRST)

Let  $ERR_j^{(p)}$  be the error reduction ratio corresponding to presynaptic neuron  $j$  at iteration  $p$  defined as

$$ERR_j^{(p)} = \frac{\left\langle s_j^{\perp(p)}, s^{y*} \right\rangle_{\mathbb{S}}^2}{\|s_j^{\perp(p)}\|_{\mathbb{S}}^2 \cdot \|s^{y*}\|_{\mathbb{S}}^2}.$$

The target output spike train  $s^{y*}$  is unknown prior to training. However, for  $y^*(t) = \pm 1$ , the inner product  $\langle s, s^{y*} \rangle_{\mathbb{S}}, \forall s \in \mathbb{S}, s = \{(a_k, t_k)\}_{k=1}^M$ , can be computed on given time interval  $[T_1, T_2]$ , representing the total simulation time, as follows

$$\begin{aligned} \langle s, s^{y*} \rangle_{\mathbb{S}} &= 2 \langle \mathcal{F}s, \mathcal{F}s^{y*} \rangle_{L^2} \\ &= 2 \langle \mathcal{F}s, y^* \rangle_{L^2} \\ &= (\pm 1) \tau_s \sum_{k=1}^M a_k \left[ e^{-\frac{\max\{T_1, t_k\} - t_k}{\tau_s}} - e^{-\frac{\max\{T_2, t_k\} - t_k}{\tau_s}} \right]. \end{aligned}$$

The algorithm for training the Readout weights and predicting the input class is given as follows.

- Initialization

- $s_j^{\perp(1)} = s_j^{out}, j = 1, \dots, N,$
- $\ell_1 = \operatorname{argmax}_{j \in \{1, \dots, N\}} ERR_j^{(1)}, L^{(1)} = \{\ell_1\},$
- $ERR_1 = ERR_{\ell_1}^{(1)},$
- $s_1^{\perp} = s_{\ell_1}^{out}, w_1^{\perp} = \frac{\langle s^{y*}, s_1^{\perp} \rangle_{\mathbb{S}}}{\|s_1^{\perp}\|_{\mathbb{S}}^2},$
- $w_1 = w_1^{\perp}.$

- For  $p = 2, \dots, N$ , compute:

- $s_j^{\perp(p)} = s_j^{\perp(p-1)} - \mathcal{P}_{s_{p-1}^{\perp}}(s_j^{out}), j \in \{1, \dots, N\} \setminus L^{(p-1)},$

where  $\mathcal{P}$  denotes the projection operator,

- $\ell_p = \operatorname{argmax}_{j \in \{1, \dots, N\} \setminus L^{(p-1)}} ERR_j^{(p)}, L^{(p)} = L^{(p-1)} \cup \{\ell_p\},$
- $ERR_p = ERR_{\ell_p}^{(p)},$
- $s_p^{\perp} = s_{\ell_p}^{out}, w_p^{\perp} = \frac{\langle s^{y*}, s_p^{\perp} \rangle_{\mathbb{S}}}{\|s_p^{\perp}\|_{\mathbb{S}}^2},$
- $a_{i,p} = \frac{\langle s_i^{out}, s_p^{\perp} \rangle_{\mathbb{S}}}{\|s_p^{\perp}\|_{\mathbb{S}}^2}, i \in \{1, \dots, p-1\},$
- $\mathbf{A}^{(p)} = \begin{bmatrix} 1 & a_{1,2} & \dots & a_{1,p} \\ 0 & 1 & \dots & a_{2,p} \\ \dots & \dots & \dots & \dots \\ 0 & 0 & \dots & a_{p-1,p} \\ 0 & 0 & \dots & 1 \end{bmatrix},$
- $\mathbf{w}^{\perp(p)} = [w_1^{\perp}, \dots, w_p^{\perp}],$

- $\mathbf{w}^{(p)} = [\mathbf{A}^{(p)}]^{-1} \mathbf{w}^{\perp(p)},$

where  $\mathbf{w}^{(p)} = [w_1^{(p)}, \dots, w_p^{(p)}]$  denote the Readout weights at iteration  $p$ ,

- $\hat{s}^{(p)} = \sum_{k=1}^p w_k^{(p)} s_{\ell_p}^{out},$

where  $\hat{s}^{(p)}$  is the Readout output,

- $Pred(\hat{s}^{(p)}) = \text{sign} \left[ T_{max} - 2\tau_s \sum_{k=1}^{M_p} a_k^{(p)} \left( e^{-\frac{T_{max}-t_k^{(p)}}{\tau_s}} - 1 \right) \right],$

where  $Pred(\hat{s}^{(p)})$  is the class prediction based on the Readout activity

on time interval  $[0, T_{max}]$ ,  $\text{sign}()$  denotes the sign function, and  $\hat{s}^{(p)} = \left\{ (a_k^{(p)}, t_k^{(p)}) \right\}_{k=1}^{M_p}.$

- Select the smallest  $p$  that gives the minimum error for validation.

## Acknowledgments

DF and DC gratefully acknowledge that this work was supported by BBSRC under grant BB/M025527/1.

## References

Billings, S. A., Chen, S., & Korenberg, M. J. (1989). Identification of MIMO non-linear systems using a forward-regression orthogonal estimator. *International journal of control*, 46 (6), 2157–2189.

Bohte, S., Kok J. & Poutr?e H.L. (2002). Errorbackpropagation in temporally encoded networks of spiking neurons. *Neurocomp*, 48 (1-4), 17–37.

Carnell, A., & Richardson, D. (2005). Linear algebra for time series of spikes. In *Proc. European Symp. on Artificial Neural Networks*.

Chen, S., Billings, S. A., & Luo, W. (1989). Orthogonal least squares methods and their application to non-linear system identification. *International Journal of Control*, 50 (5), 1873 – 1896.

Dolinský, J., Hirose, K., & Konishi, S. (2017). Readouts for echo-state networks built using locally-regularized orthogonal forward regression. *Journal of Applied Statistics*, 45 (4), 740–762.

Fabre-Thorpe, M., Richard, G., & Thorpe, S. J. (1998). Rapid categorization of natural images by rhesus monkeys. *Neuroreport*, 9 (2), 303–308.

Florescu, D. (2017). *Reconstruction, identification and implementation methods for spiking neural circuits*. Springer.

Florescu, D., & Coca, D. (2018). Identification of Linear and Nonlinear Sensory Processing Circuits from Spiking Neuron Data. *Neural Computation*, 30 (3), 670–707.

Florescu, D., & Coca, D. (2015). A novel reconstruction framework for time-encoded signals with integrate-and-fire neurons. *Neural Computation*, 27 (9), 1872–1898.

Florian, V. (2007). Reinforcement learning through modulation of spike-timing-dependent synaptic plasticity. *Neural Computation*, 19 (6), 1468–1502.

Florian, V. (2012). The Chronotron : A Neuron That Learns to Fire Temporally Precise Spike Patterns. *PloS one*, 7 (8).

Gardner, B., & Grüning, A. (2016). Supervised learning in spiking neural networks for precise temporal encoding. *PloS one*, 11 (8).

Gollisch, T., & Meister, M. (2008). Rapid neural coding in the retina with relative spike latencies. *Science*, 319 (5866), 1108–1111.

Gütig, R. (2014). To spike, or when to spike? *Current opinion in neurobiology*, 25, 134–139.

Häusler, S., & Maass, W. (2007). A statistical analysis of information-processing properties of lamina-specific cortical microcircuit models. *Cerebral cortex*, 17 (1), 149–162.

Häusler, S., Markram, H., & Maass, W. (2002). Perspectives of the high dimensional dynamics of neural microcircuits from the point of view of low dimensional readouts. *Neural Comput*, 14 (11), 2531–2560.

Hirata, Y., Katori, Y., Shimokawa, H., Suzuki, H., Blenkinsop, T. A., Lang, E. J., & Aihara, K. (2008). Testing a neural coding hypothesis using surrogate data. *Journal of neuroscience methods*, 172 (2), 312–322.

Houweling, A. R., & Brecht, M. (2008). Behavioural report of single neuron stimulation in somatosensory cortex. *Nature*, 45165–68.

Huber, D., Petreanu, L., Ghitani, N., Ranade, S., Hromádka, T., Mainen, Z., & Svoboda, K. (2008). Sparse optical microstimulation in barrel cortex drives learned behaviour in freely moving mice. *Nature*, 451, 61–64.

Hung, C. P., Kreiman, G., Poggio, T., & DiCarlo, J. J. (2005). Fast readout of object identity from macaque inferior temporal cortex. *Science*, 309 (5749), 863–866.

Izhikevich, E. M. (2006). Polychronization: Computation with Spikes. *Neural Comput*, 18 (2).

Izhikevich, E. M. (2007). Solving the distal reward problem through linkage of STDP and dopamine signaling. *Cerebral cortex*, 17 (10), 2443–2452.

Jaeger, H.(2001). The ?echo state? approach to analysing and training recurrent neural networks. Technical Report GMD Report 148, German National Research Center for Information Technology, 2001.

Jones, L. M., Depireux, D. A., Simons, D. J., & Keller, A. (2004). Robust temporal coding in the trigeminal system. *Science*, 304 (5679), 1986–1989.

Kayser, C., Montemurro, M. A., Logothetis, N. K., & Panzeri, S. (2009). Spike-phase coding boosts and stabilizes information carried by spatial and temporal spike patterns. *Neuron*, 61 (4), 597–608.

Kelly, R. C., Smith, M. A., Kass, R. E., & Lee, T. S. (2010). Local field potentials indicate network state and account for neuronal response variability. *Journal of computational neuroscience*, 29 (3), 567–579.

Kohn, A. & Smith, M. A. (2016). Utah array extracellular recordings of spontaneous and visually evoked activity from anesthetized macaque primary visual cortex (V1). *CRCNS.org*, Retrieved from: <http://dx.doi.org/10.6080/KONC5Z4X>.

Lukosevicius, M., & Jaeger, H. (2009). Reservoir Computing Approaches to Recurrent Neural Network Training. *Computer Science Review*, 3 (3), 127?-149.

Lazar, A. A., & Pnevmatikakis, E. A. (2008). Faithful Representation of Stimuli with a Population of Integrate-and-Fire Neurons. *Neural Computation*, 20 (11), 2715–2744.

Lazar, A. A., & Slutskiy, Y. B. (2015). Spiking neural circuits with dendritic stimulus processors. *Journal of Computational Neuroscience*, 38 (1): 1–24, 2015.

Maass, W., Natschläger, T., & Markram, H. (2002). Real-time computing without stable states: a new framework for neural computation based on perturbations. *Neural Comput*, 14 (11), 2531–2560.

McCulloch, W. S., & Pitts, W. (1943). A logical calculus of the ideas immanent in nervous activity. *The bulletin of mathematical biophysics.*, 5 (4), 115–133.

Mainen, Z. F., & Sejnowski, T. J. (1995). Reliability of spike timing in neocortical neurons. *Science*, 268 (5216), 1503–1506.

Markram, H., Wang, Y., & Tsodyks, M. (1998). Differential signaling via the same axon of neocortical pyramidal neurons. In *Proc. Natl. Acad. Sci.*, 95, 5323–5328.

Memmesheimer, R. M., Rubin, R., Ölveczky, B. P., & Sompolinsky, H. (2014). Learning precisely timed spikes. In *Neuron*, 82(4), 925–938.

Nicola, W., & Clopath, C. (2017). Supervised learning in spiking neural networks with FORCE training. In *Nature communications*, 8(1).

Pfister, J. P., Toyoizumi, T., Barber, D., & Gerstner, W. (2006). Optimal spike-timing-dependent plasticity for precise action potential firing in supervised learning. *Neural Comput*, 18 (6), 1318–1348.

Ponulak, F., & Kasinski, A. (2010). Supervised learning in spiking neural networks with ReSuMe: sequence learning, classification, and spike shifting. *Neural Comput*, 22 (2), 467–510.

Riehle, A., Grün, S., Diesmann, M., & Aertsen, A. (1997). Spike synchronization and rate modulation differentially involved in motor cortical function. *Science*, 278 (5345), 1950–1953.

Seth, A. K. (2015). Neural coding: rate and time codes work together. *Current Biology*, 25 (3), 357–363.

Smith, M. A.,z & Kohn, A. (2008). Spatial and temporal scales of neuronal correlation in primary visual cortex. *Journal of Neuroscience*, 28 (48), 12591–12603.

Srivastava, K. H., Holmes, C. M., Vellema, M., Pack, A. R., Elemans, C. P., Nemenman, I., & Sober, S. J. (2017). Motor control by precisely timed spike patterns. In *Proceedings of the National Academy of Sciences*, 114(5), 1171-1176.

Thomson, A. M., West, D. C., Wang, Y., & Bannister, A. P. (2002). Synaptic connections and small circuits involving excitatory and inhibitory neurons in layers 2?5 of adult rat and cat neocortex: triple intracellular recordings and biocytin labelling in vitro. *Cerebral cortex*, 12 (9), 936–953.

Vigneswaran, G., Philipp, R., Lemon, R. N., & Kraskov, A. (2013). M1 corticospinal mirror neurons and their role in movement suppression during action observation. *Curr Biol*, 23 (3).

Wolfe, J., Houweling, A. R., & Brecht, M. (2010). Sparse and powerful cortical spikes.

*Current opinion in neurobiology.*, 20 (3), 306–312.

Xu, Y., Zeng, X., Han, L., & Yang, J. (2013). A supervised multi-spike learning algo-

rithm based on gradient descent for spiking neural networks. *Neural Networks*, 43,

99–113.